A Simple Radial Gradient Filter for Batch-Processing of Coronagraph Images

Ritesh Patel[1,2,3] ⓘ **· Satabdwa Majumdar**[1,4] ⓘ **· Vaibhav Pant**[2] ⓘ **·**
Dipankar Banerjee[1,2,5] ⓘ

Abstract

Images of the extended solar corona, as observed by different white-light coronagraphs, include the K- and F-corona and suffer from a radial variation in intensity. These images require separation of the two coronal components with some additional image-processing to reduce the intensity gradient and analyse the structures and processes occurring at different heights in the solar corona within the full field of view. Over the past few decades, coronagraphs have been producing enormous amounts of data, which will be continued with the launch of new telescopes. To process these bulk coronagraph images with steep radial-intensity gradients, we have developed the algorithm *Simple Radial Gradient Filter* (SiR-GraF). This algorithm is based on subtracting a minimum background (F-corona) created using long-duration images and then dividing the resultant by a uniform-intensity-gradient image to enhance the K-corona. We demonstrate the utility of this algorithm to bring out the short-time-scale transient structures of the corona. SiRGraF can be used to reveal and analyse such structures. It is not suitable for quantitative estimations based on intensity. We have successfully tested the algorithm on images of the *Large Angle Spectroscopic COronagraph* (LASCO)-C2 onboard the *Solar and Heliospheric Observatory* (SOHO) and COR-2A onboard the *Solar TErrestrial RElations Observatory* (STEREO) with good signal-to-noise ratio (SNR) along with low-SNR images of STEREO/COR-1A and the *KCoronagraph* (KCor). We also compared the performance of SiRGraF with the existing widely used algorithm *Normalizing Radial Gradient Filter* (NRGF). We found that when hundreds of images have to be processed, SiRGraF works faster than NRGF, providing similar brightness and contrast in the images and separating the transient features. Moreover, SiRGraF works better on low-SNR images of COR-1A than on NRGF, providing better identification of dynamic coronal structures throughout the field of view. We discuss the advantages and limitations of the algorithm. The application of SiRGraF to COR-1 images can be extended for an automated coronal mass ejection (CME) detection algorithm in the future, which will help in our study of the characteristics of CMEs in the inner corona.

Keywords Corona · Corona, structures · Instrumentation and data management

1. Introduction

The observed white-light corona contains K- and F-components formed due to photospheric light scattered by free electrons and dust particles, respectively, with the later dominating

---

beyond ≈ 3 R$_\odot$ (van de Hulst, 1950; Morgan and Habbal, 2007). The shape of the white-light corona is governed by the density structures where the K-corona is associated with the magnetic-field configuration (Woo, 2005). It has been found that the F-corona remains virtually constant throughout the solar cycle at heights more than ≈ 2.6 R$_\odot$ (Morgan and Habbal, 2007). Large-scale transients, coronal mass ejections (CMEs), observed in white-light images are electron-density structures (Howard, 2011) that require a careful separation from the background (Byrne et al., 2012). A general method to separate the F-corona is subtracting the minimum intensity obtained over a long period of time (DeForest, Howard, and McComas, 2014; DeForest et al., 2018) or using a monthly minimum of daily median images (Morrill et al., 2006). Morgan and Habbal (2010) separated the transient component by estimating a background based on polynomial fitting in each radial direction. It was further developed using iterative methods for segregating the quiescent and dynamic corona while automatically detecting CMEs (Morgan, Byrne, and Habbal, 2012). Later Morgan (2015) introduced a methodology based on radiometric calibration of LASCO-C2 images to subtract the background, suppressing the noise while separating the K-corona and the dynamic structures.

One of the challenges in coronal observations, apart from separation of the two coronal components, is that due to the decreasing electron and dust particle density with height, there is a steep gradient in the observed intensity (Baumbach, 1937; van de Hulst, 1950). The radial variation of the F- and K-corona has been quantified by Morgan and Habbal (2007) over different phases of the solar cycle. The analysis using coronagraph images becomes challenging unless some image-processing technique is used to reduce the brightness variation. Various methods in the form of a radial-gradient filter (RGF) have been developed to overcome this difficulty. In this regard, RGF-based photography was made using a mechanical rotating sector to image the corona (Owaki and Saito, 1967), or a radial-density filter was placed in the optical path of an imaging instrument to photograph solar eclipses (Newkirk and Harvey, 1968). Solar-eclipse photographs were made as composite images, combining multiple exposure frames for the process. To enhance the high dynamic range of brightness in the corona during such an event, different image-processing techniques were developed (Koutchmy et al., 1992; Espenak, 2000; Druckmüller, Rušin, and Minarovjech, 2006). These techniques enhance the structures with high spatial frequencies leading to the visibility of sharp features in the images. To identify the CMEs in the midst of such dynamic coronal intensity, Byrne et al. (2009) introduced a method based on multiscale filtering, thereby enhancing the visibility of CMEs.

Morgan, Habbal, and Woo (2006) introduced the normalising-radial-gradient filter (NRGF), which subtracts the mean intensity followed by division by the standard deviation at each height to reduce the radial-intensity variation. This method has been extensively used to enhance coronal structures with applications to eclipse images (Pasachoff et al., 2007; Habbal et al., 2010, 2011; Boe et al., 2018), automated detection of CMEs using the *Coronal Image Processing* (CORIMP) technique (Byrne et al., 2012; Morgan, Byrne, and Habbal, 2012), Automated CME Triangulation (Hutton and Morgan, 2017), identification of plasmoids in the corona (Lee et al., 2020; Patel et al., 2020), and identification of Alfvén waves in the solar atmosphere (He et al., 2009). An improvement of this algorithm was developed, known as the *Fourier normalising-radial-graded filter* (FNRGF), based on finite Fourier series that takes a local average and standard deviation, and this was used to enhance fine coronal structures in the low-contrast regions (Druckmüllerová, Morgan, and Habbal, 2011). Recently, a new method, called the *radial local multiscale filter* (RLMF), was developed using multiscale filtering on radial vectors extracted from corona-graph images followed by intensity normalisation leading to enhancement of coronal struc-

tures (Qiang et al., 2020). For the detection of inbound waves in the solar corona, DeForest, Howard, and McComas (2014) normalised the radial intensity of the COR-2 images by subtracting the average intensity across a column and time from each row, followed by dividing each row by its standard deviation across column and time.

Methods based on wavelets to enhance coronal features in extreme ultraviolet (EUV) images were developed by Stenborg and Cobelli (2003) and Stenborg, Vourlidas, and Howard (2008). To enhance the off-disk coronal structures in EUV images of the *Atmospheric Imaging Assembly* (AIA: Lemen et al., 2012) by improving the intensity variation radially, IDL routines aia_rfilter.pro and aia_rfilter_jp2gen.pro were developed (see aia.cfa.harvard.edu/software.shtml). These add the off-limb component of many AIA images thereby increasing the signal-to-noise ratio (SNR). The off-disk corona is then further divided into concentric rings, which are scaled as functions of their radial distance, average intensity, and the intensity with respect to rings in the neighborhood (Masson et al., 2014). EUV coronal structures were also enhanced while reducing the dominance of noise based on a fuzzy algorithm (Druckmüller, 2013) and using Gaussian filtering for bringing out features at different scales (Morgan and Druckmüller, 2014). In another algorithm, *CMEs Identification in Inner Solar Corona* (CIISCO), a radial filter was applied on EUV images by dividing each individual image by a background uniform in azimuthal direction generated using the radial-intensity profile of the polar regions of the Sun (Patel et al., 2021).

Each of the above-mentioned algorithms has its own advantages and limitations. Even though all of these succeed in enhancing the coronal structures and reducing the intensity variation, the processing time becomes large when the number of images to be analysed becomes large. Bulk image processing is required for such cases; some of that include long-term study of CMEs and long-term study of solar corona (Lamy et al., 2020, 2021). Therefore in this article, we present the *Simple Radial Gradient Filter* (SiRGraF) algorithm, which works faster when hundreds of images have to be processed to reveal the dynamic coronal features. The article is arranged as follows: The algorithm is introduced in Section 2, and the results of the application of SiRGraF on coronagraph images and comparison with NRGF in Section 3. We summarise our work and discuss the analysis in Section 4.

2. Algorithm

The observations of the white-light corona in coronagraph images exhibit a steep outward decrease in intensity (van de Hulst, 1950; Morgan, Habbal, and Woo, 2006; Morgan and Habbal, 2007). To analyse coronagraph images and study the associated physical processes, specially transient activities in detail, it is important to identify the coronal features throughout the FOV. In this work, we have used the Level-1 images of the white-light coronagraphs including the *Large Angle Spectrometric Coronagraph* (LASCO: Brueckner et al., 1995) onboard the *Solar and Heliospheric Observatory* (SOHO), *Sun Earth Connection Coronal and Heliospheric Investigation* (SECCHI: Howard et al., 2008) of the *Solar Terrestrial Relations Observatory* (STEREO), and the *KCoronagraph* (KCor: de Wijn et al., 2012) of the Mauna Loa Solar Observatory (MLSO). The Level-1 images are the total-brightness images calibrated to the mean solar-disk brightness, flat and dark-corrected with alignment and with corrections done for solar North up. In the following steps, we demonstrate the methodology involved in the SiRGraF using Level-1 STEREO/COR-1A data of 01 August 2010 taken at a cadence of five minutes:

i) Level-1 images [I] of a single day are taken to produce a single image, called the minimum background [I_m], as shown in Figure 1a. This is generated such that each pixel in

(a)

(b)

(c)

(d)
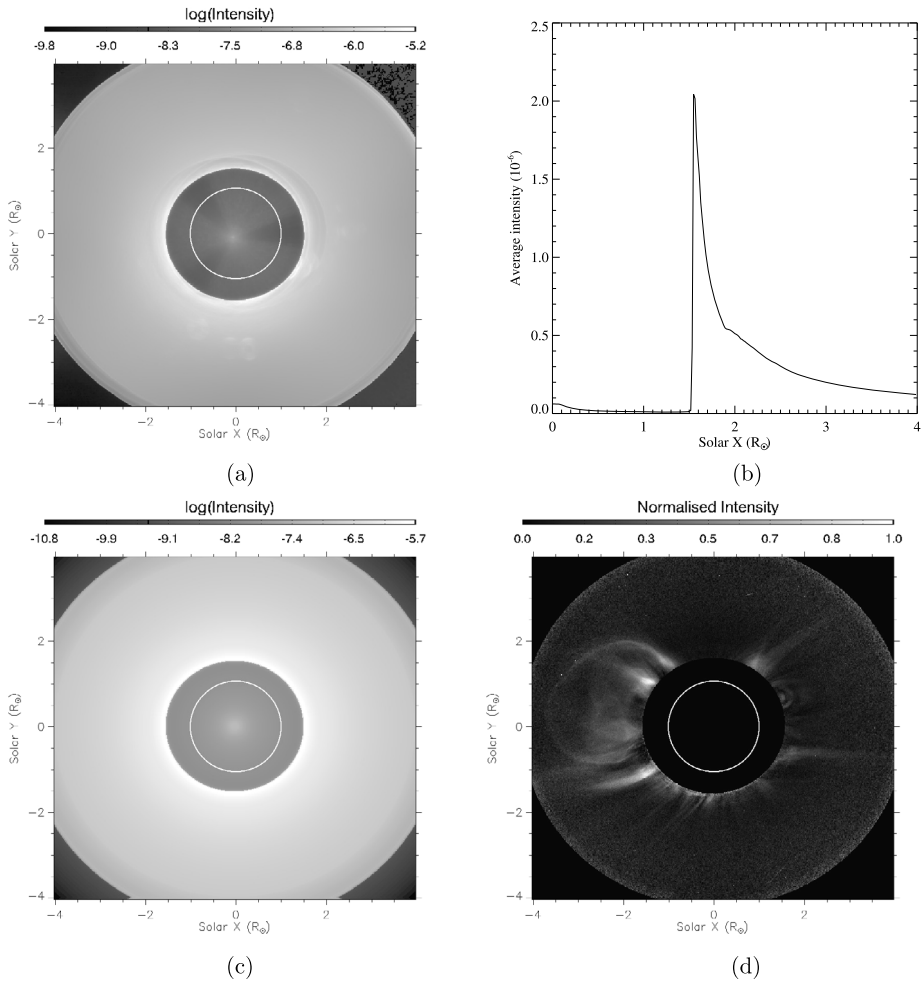
Figure 1 An outline of the SiRGraF algorithm on application to images of STEREO/COR-1A observed on 01 August 2010. (**a**) Minimum background image created from Level-1 images of whole day. (**b**) Azimuthal average radial-intensity plot generated from the minimum background image. (**c**) A circularly symmetric uniform background generated from the radial-intensity array of (**b**). (**d**) Final image at 08:27 UT after subtracting the minimum background and dividing the resultant image by the uniform background. The intensity in (**a**) and (**c**) are displayed on a log scale, whereas the normalised intensity is displayed in (**d**).

I_m corresponds to the minimum intensity (with intensity greater than zero to avoid the outliers) of all the images. This image consists of intensity from F-corona, less variable K-corona, and instrumental scattered light (Morgan and Habbal, 2007). The minimum background is taken instead of the 1 percentile minimum to make the processing fast and efficient.

ii) This minimum background is used to generate a radial-intensity profile such that the intensity at a certain height is the average of all intensities in the azimuthal direction at that height (Figure 1b). This smooths out the variation intensity in the azimuthal direction. As a one-day minimum background is used here, the presence or absence

of long-lived streamers may contribute at those distances above the limb, which gets averaged out while creating the radial 1D-profile.

iii) The radial profile is then incorporated to produce a uniform-background image [I_u] with a circularly symmetric intensity gradient. Figure 1c shows a uniform-background image made using the radial profile shown in Figure 1b. As the instrument background and scatter remains nearly uniform from the Equator to polar regions (Morgan and Habbal, 2007; Patel et al., 2018), this will serve to normalising such contributors of the radial gradient along with inherent coronal-intensity variation.

iv) After obtaining the background images, the Level-1 images are thereby filtered for the radial-intensity gradient using the following relation:

$$I' = \frac{I - I_m}{I_u}. \tag{1}$$

Equation 1 represents the core of the SiRGraF. The numerator shows the removal of the static and quasi-static components of the corona along with instrumental background bringing out the K-corona. This minimum background subtraction is in contrast with the pipeline of the LASCO and STEREO coronagraphs, where monthly minimum background of daily median images are used as background. One should note that the daily median image has a contribution from K-corona more than the daily minimum image (Thompson et al., 2010). For the objective of separating the dynamics and transients (CMEs), it is required to capture the maximum part of the K-corona signal. When the K-corona obtained after removing the background is divided by a uniform background, the radial variation of intensity is reduced, thereby allowing visualisation of coronal structures to greater heights uniformly in the azimuthal direction. The filtered images with normalised intensities will thus visibly exhibit coronal structures as shown in Figure 1d. The use of single-day minimum background brings out the more dynamic components of the K-corona, which in this case are the CMEs and dynamically changing streamers as seen in Figure 1d. The streamers on this day were either displaced by the CMEs or short-lived making them dynamic in nature. The use of a extended-period minimum background could bring out long-lived structures of the corona, which could not be extracted in the example presented here.

3. Results

3.1. Application to Coronagraph Images

An application of SiRGraF to STEREO/COR-1A images is illustrated in Figure 1. We also tested the algorithm on Level-1 images of other white-light coronagraphs of LASCO-C2, STEREO/COR-2A, and MLSO/KCor. Figure 2 shows such an example, where the top panel shows radial-filtered LASCO-C2 images of 07 January 2001 using SiRGraF. The backgrounds for the space-based coronagraphs have been prepared using the available whole-day images. We can see that the different parts of the classic three-part-structured CME have been brought out clearly by SiRGraF throughout the FOV. It should be noted that an example of this CME using NRGF has been presented by Morgan, Habbal, and Woo (2006) and a direct comparison could be made in the two processes. The middle panel of the same figure shows filtered successive images of STEREO/COR-2A of 01 August 2010, which is the same CME example taken for COR-1A. For this instrument, CME and other coronal structures can be distinctly identified to considerably larger heights. We can also notice faint rings near the outer edge of the FOV in COR-2A images. These rings are due to increased
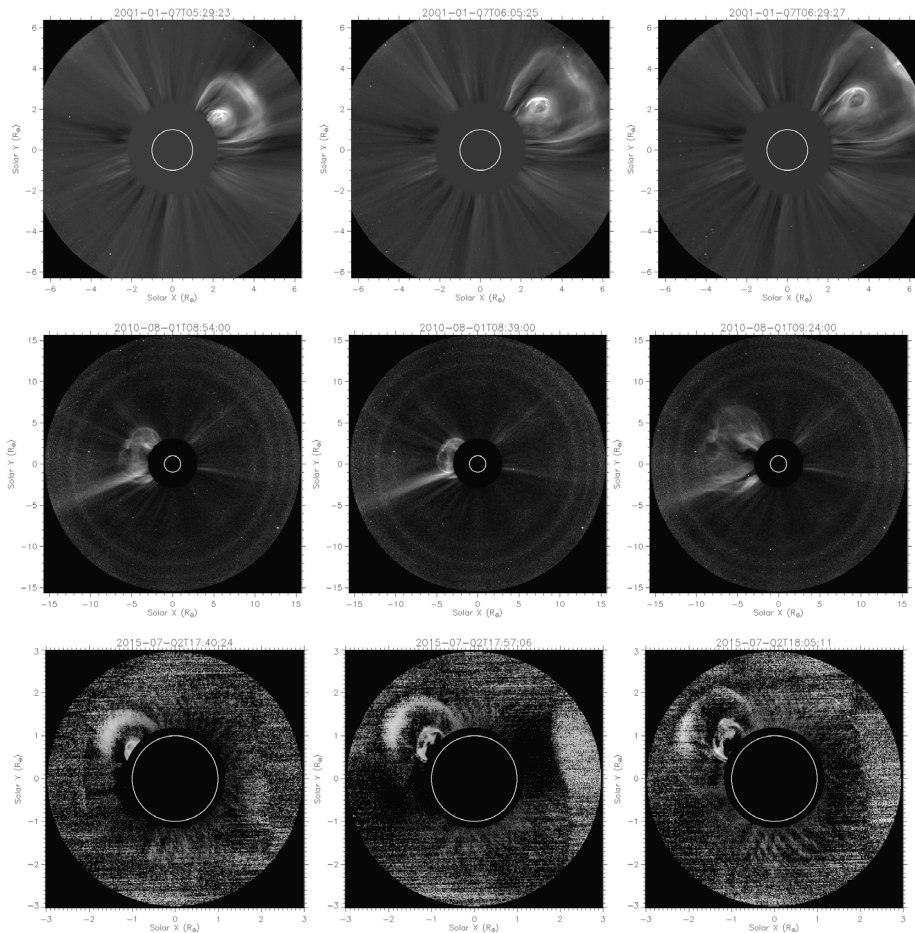
Figure 2 Application of SiRGraF on successive images of LASCO-C2 taken on 07 July 2001, STEREO/COR-2A taken on 01 August 2010, and KCor taken on 02 July 2015, respectively, in *top, middle, and bottom panels*. Different parts of the CME and coronal structures can be clearly seen to the outer edge of FOV for C2 and COR-2A images and only CME structures in KCor images. The images are displayed with normalised intensity.

photon noise near the outer vignetting minimum of the instrument (DeForest et al., 2018). These rings have intensity greater than the backgrounds that we have used for filtering and hence are visible in the processed images. Note that these are of instrumental origin, and advanced processing will be required to remove these artifacts (DeForest et al., 2018).

We also applied this algorithm to Level-1 images of KCor taken on 02 July 2015 with a cadence of 15 seconds. As KCor is a ground-based coronagraph, we employed only the limited hours of observed data available for this day to create the required backgrounds. In the bottom panel of Figure 2 the output after the implementation of the algorithm can be seen in KCor images for three instances. It can be seen that in spite of the atmospheric contributions, the different parts of the CME can be identified almost to the outer edge of the FOV. Such enhancement is achieved without the need to add the images to improve the SNR or compromising on the cadence. KCor being a ground-based coronagraph, the minimum background
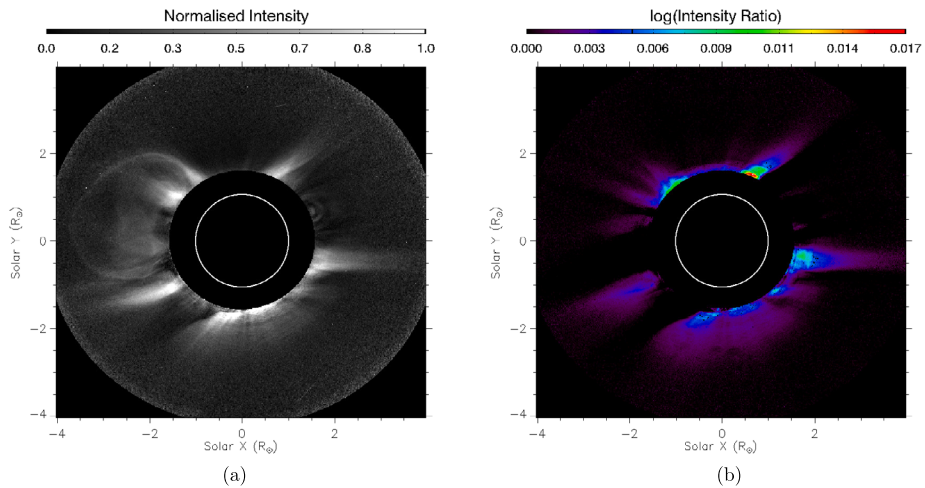
Figure 3 (**a**) COR-1A image of 01 August 2010 at 08:27 UT processed with SiRGraF using background created with seven-day intensity images. (**b**) Intensity ratio of minimum backgrounds using one-day and seven-day images.

suffers from atmospheric contamination and hence could not be obtained as clearly as for space-based coronagraphs. As a result, the signatures of the streamers are lost for this case, limiting SiRGraF to mostly space-based coronagraph images and to only analysis involving erupting structures for ground-based coronagraph images. A longer period (ten days to one month) for minimum background creation could be considered for the KCor in the future for significantly bringing out the signal of streamer-like long-lived structures.

3.2. Comparison with Extended Period Background

We also created a seven-day background to identify the effects of long-period background while processing the coronagraph images. We used total-brightness images from 26 July 2010 to 01 August 2010 to process the COR-1A images of 01 August 2010. The minimum background was created using this extended period of data, and the uniform background was obtained based on this minimum image as mentioned in Section 2. Figure 3a shows the output of the algorithm after application. When it is compared with Figure 1d, we can see that the transient CME is brought out clearly in both cases. In addition to CMEs, the streamers are more distinctly visible when an extended background is used in the algorithm. The streamers located near the north-west and western limb of the Sun are more pronounced, as suggested in Section 2.

We also compared the intensities of the minimum background created using one-day and seven-day images for the same dataset (Figure 3b). We can notice that the background plays a small role for the majority of the regions where a CME is present. The ratio suggests that an increased contribution from streamers is present for a single-day background in comparison with the seven-day case. Hence it is also reflected in the processed images. Even though this ratio only accounts for $\approx 5\%$ difference in the background determination, its effect can be seen when long-lived structures such as streamers are considered. We need to identify the science target while considering the period for creating the backgrounds.

3.3. Comparison with NRGF

The SiRGraF algorithm uses Equation 1, whereas NRGF is based on the following relation:

$$I_{\text{filt}}(r, \phi) = \frac{I(r, \phi) - I(r)_{\langle \phi \rangle}}{\sigma(r)_{\langle \phi \rangle}}, \tag{2}$$

where $I_{\text{filt}}(r, \phi)$ is the NRGF processed image, $I(r, \phi)$ is the original intensity image at height r and position angle ϕ, and $I(r)_{\langle \phi \rangle}$ and $\sigma(r)_{\langle \phi \rangle}$ are the average and standard deviation of the intensities at the height r computed over all position angles. On comparing Equations 1 and 2, we see that SiRGraF performs matrix operation using the two backgrounds (minimum and maximum) at a given time, whereas NRGF performs row-wise operation requiring the computation of the mean and standard deviation at each height at a given time. Both of these methods subtract an average intensity, which is then normalised to flatten the radial-intensity variation. We used 339 Level-1 total brightness images of STEREO/COR-1A of size 512×512 pixels and processed with SiRGraF and NRGF on an i7 computer with a base clock speed of 1.8 GHz and 8 GB of RAM. The application of SiRGraF is based on the steps mentioned in Section 2, where the backgrounds are created using all 339 images. We used the IDL routine nrgf.pro to process the images with NRGF.

We found that SiRGraF takes a comparatively longer time (≈ 2.5 seconds) to process a single image, whereas NRGF takes only a fraction of a second. This is because the two backgrounds that need to be generated for SiRGRaF take the majority of the time in the process. At the same time, it should also be kept in mind that SiRGraF produces images where the coronal features are visually identified with relatively better clarity and ease. When the whole batch of 339 images is processed by the two filters, SiRGraF takes ≈ 3 seconds to complete the whole process similar to NRGF when the inputs to Equation 2 are kept constant over the batch of images. This defines the efficiency of this algorithm when hundreds of images have to be processed. We used the Michelson contrast ratio (Michelson, 1927) to compare the intensity contrast in processed images. This parameter is defined as

$$V = \frac{I_{\text{max}} - I_{\text{min}}}{I_{\text{max}} + I_{\text{min}}}, \tag{3}$$

where I_{max} and I_{min} are the maximum and minimum intensities in the image. We measured the contrast in individual images and then averaged for the whole batch. It turns out that the mean contrast produced by the two methods is close to unity, and hence they are very similar in nature.

After going through the quantitative assessments of the two methods, we looked for the visual differences in the outputs of the two. An animation is also available with Figure 4, providing a side-by-side comparison of SiRGraF with NRGF applied to COR-1A images. On comparing Figure 4 with Figure 1d visually along with the animation, we found that both SiRGraf and NRGF reveal the coronal structures up to the outer edge of FOV in the images. We noticed that SiRGraF-processed COR-1 images appear to be uniformly illuminated as compared to the NRGF ones. In NRGF-processed images, the features in the inner FOV appear brighter than those at the outer edges. Due to this, the structures at the inner FOV in NRGF processed images are not distinctly visible when compared with SiRGraF processed ones.

Figure 4 Output of application of NRGF on COR-1A image of 01 August 2010 08:27 UT. An animation is available in the Electronic Supplementary Material.
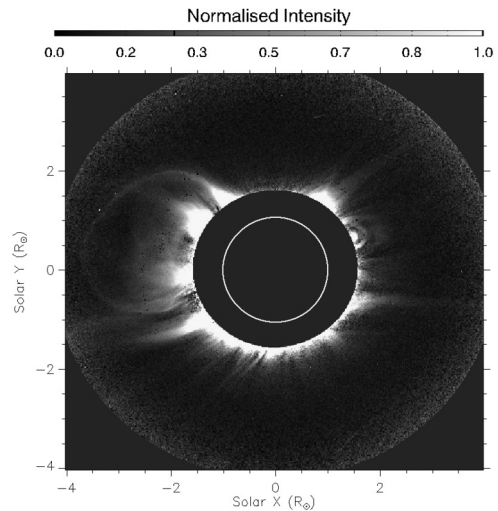

3.4. Solar-Cycle Variations

We have applied SiRGraF to different datasets including LASCO-C2, STEREO/COR-1A and COR-2A, and KCor with observations covering different phases of the solar cycle. Figure 1 shows the output of the algorithm when applied to COR-1A images near the minimum of Solar Cycle 24. The result is also compared with the outcome of NRGF images in Figure 4. We also tested SiRGraF on COR-1A images for the observations of 03 April 2014 during the maximum phase of the solar cycle. The COR-1 images have resulted in poor SNR over the years with an uncertain jitter pattern in the images and hence degrading the image quality over Solar Cycle 24 (see cor1.gsfc.nasa.gov/docs/COR1_status.pdf). Application to such images with poor SNR served as a crucial test for our algorithm. This was also compared with application of NRGF on the same set of images as shown in Figure 5. The output of SiRGraF is in the left panel, whereas NRGF is shown on the right. Both algorithms appear to work similarly for the COR-1A images observed during the solar maximum. It is evident that the inner FOV appears brighter for NRGF images as compared to SiRGraF output, and this has already been mentioned in Section 3.3. As a result, a difference can be observed in identification of the structures close to the inner FOV. The first appearance of the CME in the top panel appears to be obscured by the intensity in the NRGF-processed images, whereas the CME can be clearly seen for SiRGraF-filtered images. This is an essential requirement for the study of kinematics of CMEs at the lower heights with only white-light observations. Any discrepancy in the identification of a tracked feature at the lower heights might result in missing the impulsive acceleration phase, or an erroneous measurement can lead to spurious results. The evolution of the CME through the FOV can be seen in successive frames. It is observed that SiRGraF provides a uniform identification of different structures of the CME at all the heights, unlike NRGF. This could serve as an important application of our algorithm on COR-1 images enabling us to better observe CMEs close to the Sun. The usefulness of both of these algorithms is limited to the lower heights because the SNR becomes low toward the outer edge of the FOV (beyond $\approx 3.5\ R_\odot$) in COR-1 images, as it is evident in both cases.

For the COR-1A images observed during solar maxima and minima and processed with SiRGraF, we compared the radial variation in the intensity at all of the position angles (PAs)
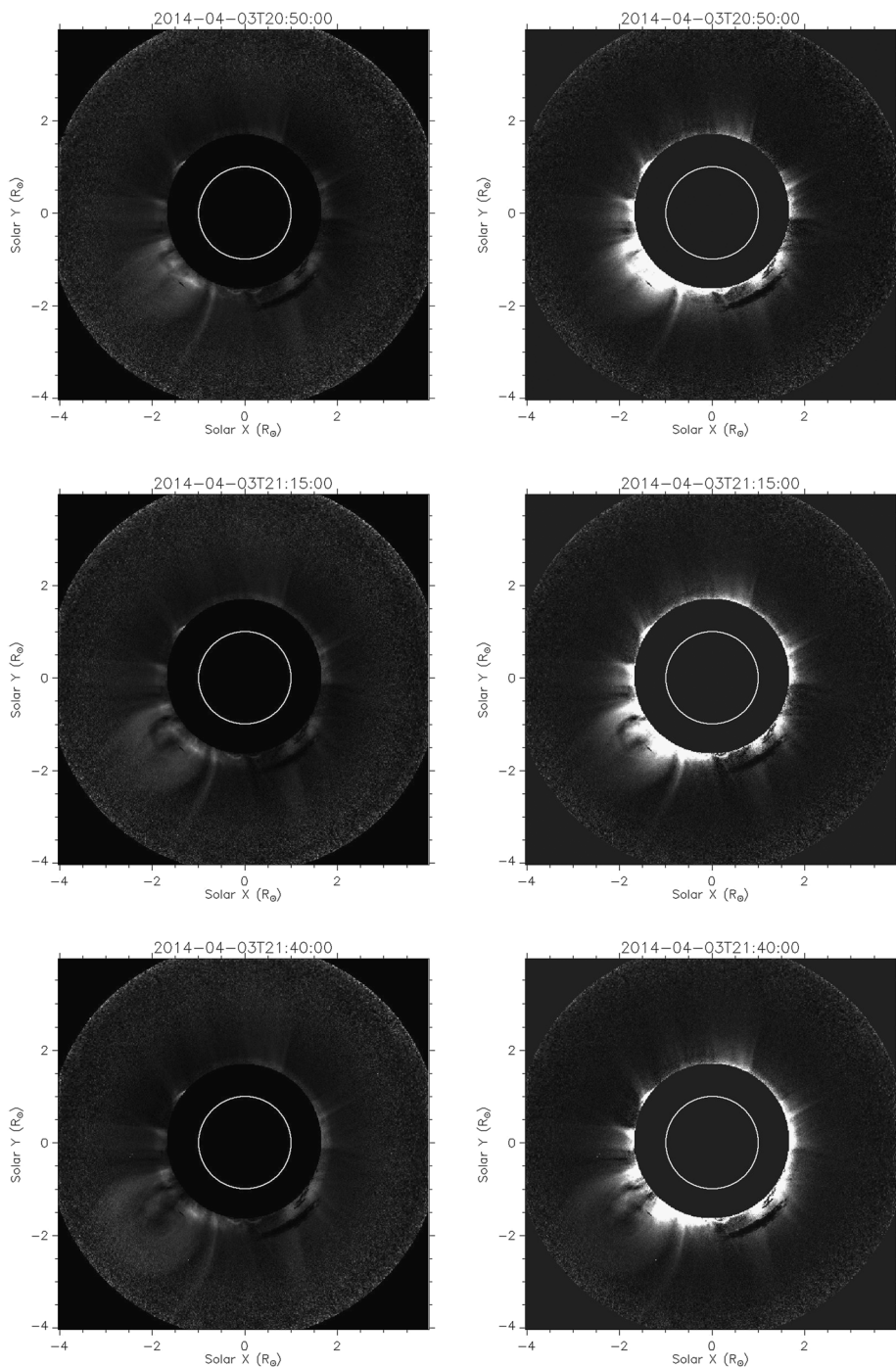
Figure 5 A comparison of application of SiRGraF (*left panels*) and NRGF (*right panels*) on images of STEREO/COR-1A observed at the maximum period of the solar cycle on 03 April 2014. (An animation is available in the Electronic Supplementary Material.)
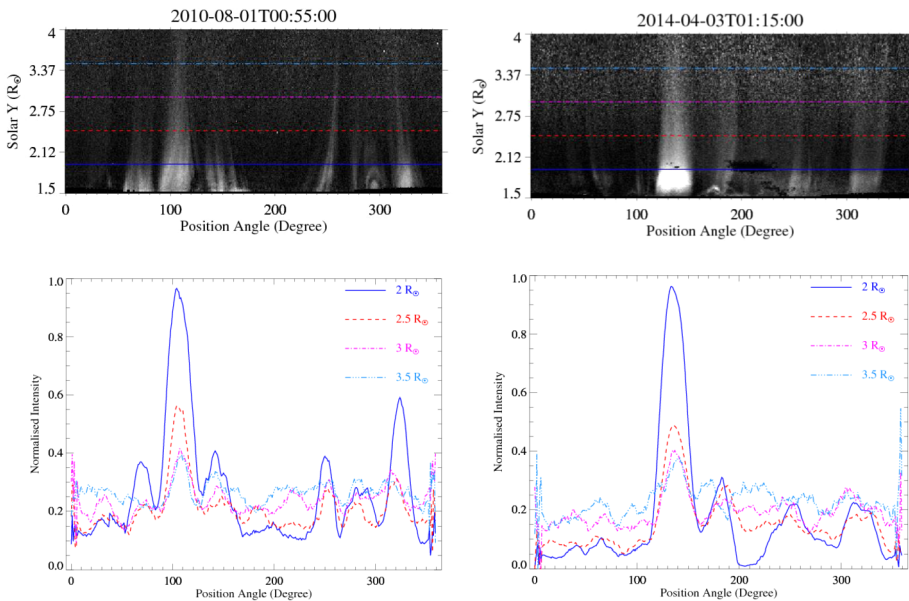
Figure 6 Radial-intensity variation after the application of SiRGraF to COR-1A images taken during solar minima (*left*) and maxima (*right*). The *upper panel* shows the images converted to polar coordinates, whereas the *lower panel* shows the normalised intensities at the four heights marked in the images of the upper panel.

as shown in Figure 6. The top panel shows the images taken at the two phases of the solar cycle converted to polar coordinates, whereas the bottom panel shows the normalised intensity variations at the four heights marked in the top panel. We can see that for both images, the intensities in the processed images are close to each other at all the heights except at the bright-streamer regions. In the intensity plot for 03 April 2014 image, there is a sharp dip in the intensity at 2 $R_\odot$ at PA of $\approx 200°$. It should be noted that at this particular location, there is some dark artifact in the corresponding image shown in the top panel, which is responsible for this dip. Other regions with fewer structures do not show a steep change in intensity from inner to outer FOV for both images. The performance of the algorithm on the images observed during different phases of the solar cycle enhances its utility for studying the coronal dynamics over long periods.

4. Summary

To study the dynamics of the solar atmosphere using coronagraph images, it is important to well visualise the structures throughout the FOV. The radial gradient in the intensity of the corona makes it difficult to observe the structures throughout the FOV with same brightness and contrast in the images. To reduce the radial gradient in the intensity in such huge number of images in a faster manner and bring out the details of coronal transients, we have developed the algorithm *Simple Radial Gradient Filter* (SiRGraF). The algorithm requires two backgrounds for processing a coronagraph image: One is a minimum-background image prepared from at least a day of images to filter out the constant background, and the other one is a uniform-intensity circularly symmetric background prepared using the azimuthal average radial-intensity profile from the minimum background. The minimum background

is subtracted from individual images followed by division of the difference image by the uniform background. The images processed with this filter appear to show identification of the coronal structures throughout the coronagraph FOV with uniform intensity. We found that this algorithm works well in identifying the coronal structures in the coronagraph images over different phases of the solar cycle. These include the ones with good SNR, such as LASCO-C2 and STEREO/COR-2A, and poor SNR images of STEREO/COR-1A and KCor. We illustrated the effect of different periods of background used in the SiRGraF, which shows for transients such as CMEs that the one-day backgrounds perform in a similar way as the extended period one. The same is not applicable while considering long-lived streamers.

We also compared the performance of our algorithm with NRGF and found that SiR-GraF is efficient and fast when a large number of coronagraph images have to be processed quickly. The processing time of SiRGraF could be further reduced by using the minimum backgrounds, which have already been generated for instruments such as STEREO/COR-1. In addition, if uniform backgrounds could also be stored in a similar way, then SiRGraF would work even faster for bulk processing of images. This performance of SiRGraF is achieved maintaining the intensity contrast similar to NRGF. We notice in Figure 5 that a faint halo is observed in SiRGraF-processed images, which is present neither in the NRGF ones nor in Figure 1. During the period of observation considered in the solar-maxima case, STEREO/COR-1A is associated with high jitter and instrument-related artifacts. Upon careful observation, we found that the presence of rogue nonzero-intensity values near the southwest limb outside the occulter has contributed to the background creation, which is reflected as a halo in the filtered images. This does not impact the identification and tracking of CMEs in subsequent images, but it will be taken care of in a future version of the algorithm. One needs to be careful when implementing this algorithm and generating the backgrounds for data when roll maneuvers are performed for the SOHO and STEREO spacecraft where the FOV of the instruments are rotated.

This kind of processing could be used while studying the kinematics and morphology of CMEs over long periods of time. One should be careful when using this data product to estimate the CMEs mass. Such estimations require accurate intensity measurements that get flattened out in the radial-filtering process. It should be noted that among the existing white-light coronagraphs, STEREO/COR-1 observes the inner corona closest down to 1.4 $R_\odot$ and KCor down to 1.05 $R_\odot$. The application of SiRGraF on large amounts of COR-1 and KCor data could provide us an improvement in understanding the CME dynamics in the inner corona. Moreover, it could also pave a path for the development of an automated CME-detection algorithm to work well with COR-1 and KCor images and generate statistics of CME properties during their early evolution. Processing COR-1 and KCor images with SiRGraF will also be useful as inputs to stereoscopic forward modeling using Graduated Cylindrical Shell (Thernisien, Howard, and Vourlidas, 2006; Thernisien, Vourlidas, and Howard, 2009; Thernisien, 2011; Majumdar et al., 2020). The application of the algorithm is not only limited to CMEs, but also to analysing the dynamics of streamers, blobs, current sheets/rays, etc. in this FOV and long-term coronal studies (Lamy et al., 2020, 2021). The recently launched *Multi-Element Telescope for Imaging and Spectroscopy* (METIS) onboard *Solar Orbiter* (Müller et al., 2020) and future space-based missions, including the *Visible Emission Line Coronagraph* (VELC: Raghavendra Prasad et al., 2017; Banerjee, Patel, and Pant, 2017) onboard *Aditya-L1* (Seetha and Megala, 2017) and the *Association of Spacecraft for Polarimetric and the Imaging Investigation of the Corona of the Sun* (ASPIICS: Renotte et al., 2014) of the *Project for Onboard Autonomy-3* (PROBA-3), will also observe the inner corona. The application of SiRGraF to their data will be helpful to bring out processes occurring in the inner corona, thereby improving our understanding of the same.

Data Availability The datasets generated during the current study are available from the corresponding author on reasonable request.

Declarations

Conflict of Interest The authors declare that they have no conflict of interests.

References

Banerjee, D., Patel, R., Pant, V.: 2017, The inner coronagraph on board ADITYA-L1 and automatic detection of CMEs. In: Foullon, C., Malandraki, O. (eds.) *Space Weather of the Heliosphere: Processes and Forecasts*, *Proc. Internat. Astron. Union Sympos.* **335**, Cambridge University Press, Cambridge, 340. DOI.

Baumbach, S.: 1937, Strahlung, Ergiebigkeit und Elektronendichte der Sonnenkorona. *Astron. Nachr.* **263**, 121. DOI.

Boe, B., Habbal, S., Druckmüller, M., Landi, E., Kourkchi, E., Ding, A., Starha, P., Hutton, J.: 2018, The first empirical determination of the Fe^{10+} and Fe^{13+} freeze-in distances in the solar corona. *Astrophys. J.* **859**, 155. DOI. ADS.

Brueckner, G.E., Howard, R.A., Koomen, M.J., Korendyke, C.M., Michels, D.J., Moses, J.D., Socker, D.G., Dere, K.P., Lamy, P.L., Llebaria, A., Bout, M.V., Schwenn, R., Simnett, G.M., Bedford, D.K., Eyles, C.J.: 1995, The Large Angle Spectroscopic Coronagraph (LASCO). *Solar Phys.* **162**, 357. DOI. ADS.

Byrne, J.P., Gallagher, P.T., McAteer, R.T.J., Young, C.A.: 2009, The kinematics of coronal mass ejections using multiscale methods. *Astron. Astrophys.* **495**, 325. DOI. ADS.

Byrne, J.P., Morgan, H., Habbal, S.R., Gallagher, P.T.: 2012, Automatic detection and tracking of coronal mass ejections. II. Multiscale filtering of coronagraph images. *Astrophys. J.* **752**, 145. DOI. ADS.

de Wijn, A.G., Burkepile, J.T., Tomczyk, S., Nelson, P.G., Huang, P., Gallagher, D.: 2012, Stray light and polarimetry considerations for the COSMO K-coronagraph. In: Stepp, L.M., Gilmozzi, R., Hall, H.J. (eds.) *Ground-Based and Airborne Telescopes IV*, *Proc. Soc. Photo-Opt. Instrum. Eng. (SPIE)* **8444**, 84443N. DOI. ADS.

DeForest, C.E., Howard, T.A., McComas, D.J.: 2014, Inbound waves in the solar corona: A direct indicator of Alfvén surface location. *Astrophys. J.* **787**, 124. DOI. ADS.

DeForest, C.E., Howard, R.A., Velli, M., Viall, N., Vourlidas, A.: 2018, The highly structured outer solar corona. *Astrophys. J.* **862**, 18. DOI. ADS.

Druckmüller, M.: 2013, A noise adaptive fuzzy equalization method for processing solar extreme ultraviolet images. *Astrophys. J. Suppl.* **207**, 25. DOI. ADS.

Druckmüller, M., Rušin, V., Minarovjech, M.: 2006, A new numerical method of total solar eclipse photography processing. *Contrib. Astron. Obs. Skaln. Pleso* **36**, 131. ADS.

Druckmüllerová, H., Morgan, H., Habbal, S.R.: 2011, Enhancing coronal structures with the Fourier normalizing-radial-graded filter. *Astrophys. J.* **737**, 88. DOI.

Espenak, F.: 2000, Digital compositing techniques for coronal imaging (invited review). In: Livingston, W., Özgüç, A. (eds.) *Last Total Solar Eclipse of the Millennium* **CS-205**, Astron. Soc. Pacific, San Francisco, 101. ADS.

Habbal, S.R., Druckmüller, M., Morgan, H., Daw, A., Johnson, J., Ding, A., Arndt, M., Esser, R., Rušin, V., Scholl, I.: 2010, Mapping the distribution of electron temperature and Fe charge states in the corona with total solar eclipse observations. *Astrophys. J.* **708**, 1650. DOI. ADS.

Habbal, S.R., Druckmüller, M., Morgan, H., Ding, A., Johnson, J., Druckmüllerová, H., Daw, A., Arndt, M.B., Dietzel, M., Saken, J.: 2011, Thermodynamics of the solar corona and evolution of the solar magnetic field as inferred from the total solar eclipse observations of 2010 July 11. *Astrophys. J.* **734**, 120. DOI. ADS.

He, J.-S., Tu, C.-Y., Marsch, E., Guo, L.-J., Yao, S., Tian, H.: 2009, Upward propagating high-frequency Alfvén waves as identified from dynamic wave-like spicules observed by SOT on Hinode. *Astron. Astrophys.* **497**, 525. DOI. ADS.

Howard, T.: 2011, *Coronal Mass Ejections: An Introduction*, *Astrophys. Space Sci. Lib.* **376**, Springer, Cham. DOI. ADS.

Howard, R.A., Moses, J.D., Vourlidas, A., Newmark, J.S., Socker, D.G., Plunkett, S.P., Korendyke, C.M., Cook, J.W., Hurley, A., Davila, J.M., Thompson, W.T., St. Cyr, O.C., Mentzell, E., Mehalick, K., Lemen, J.R., Wuelser, J.P., Duncan, D.W., Tarbell, T.D., Wolfson, C.J., Moore, A., Harrison, R.A., Waltham, N.R., Lang, J., Davis, C.J., Eyles, C.J., Mapson-Menard, H., Simnett, G.M., Halain, J.P., Defise, J.M., Mazy, E., Rochus, P., Mercier, R., Ravet, M.F., Delmotte, F., Auchere, F., Delaboudiniere, J.P., Bothmer, V., Deutsch, W., Wang, D., Rich, N., Cooper, S., Stephens, V., Maahs, G., Baugh, R., McMullin, D., Carter, T.: 2008, Sun Earth Connection Coronal and Heliospheric Investigation (SECCHI). *Space Sci. Rev.* **136**, 67. DOI. ADS.

Hutton, J., Morgan, H.: 2017, Automated detection of coronal mass ejections in three-dimensions using multi-viewpoint observations. *Astron. Astrophys.* **599**, A68. DOI. ADS.

Koutchmy, S., Altrock, R.C., Darvann, T.A., Dzubenko, N.I., Henry, T.W., Kim, I., Koutchmy, O., Martinez, P., Nitschelm, C., Rubo, G.A.: 1992, Coronal photometry and analysis of the eclipse corona of July 22, 1990. *Astron. Astrophys. Suppl. Ser.* **96**, 169. ADS.

Lamy, P., Llebaria, A., Boclet, B., Gilardy, H., Burtin, M., Floyd, O.: 2020, Coronal photopolarimetry with the LASCO-C2 coronagraph over 24 years [1996 - 2019]. *Solar Phys.* **295**, 89. DOI. ADS.

Lamy, P., Gilardy, H., Llebaria, A., Quémerais, E., Ernandez, F.: 2021, LASCO-C3 observations of the K- and F-coronae over 24 years (1996–2019): Photopolarimetry and electron density distribution. *Solar Phys.* **296**, 76. DOI. ADS.

Lee, J.-O., Cho, K.-S., Lee, K.-S., Cho, I.-H., Lee, J., Miyashita, Y., Kim, Y.-H., Kim, R.-S., Jang, S.: 2020, Formation of post-CME blobs observed by LASCO-C2 and K-Cor on 2017 September 10. *Astrophys. J.* **892**, 129. DOI. ADS.

Lemen, J.R., Title, A.M., Akin, D.J., Boerner, P.F., Chou, C., Drake, J.F., Duncan, D.W., Edwards, C.G., Friedlaender, F.M., Heyman, G.F., Hurlburt, N.E., Katz, N.L., Kushner, G.D., Levay, M., Lindgren, R.W., Mathur, D.P., McFeaters, E.L., Mitchell, S., Rehse, R.A., Schrijver, C.J., Springer, L.A., Stern, R.A., Tarbell, T.D., Wuelser, J.-P., Wolfson, C.J., Yanari, C., Bookbinder, J.A., Cheimets, P.N., Caldwell, D., Deluca, E.E., Gates, R., Golub, L., Park, S., Podgorski, W.A., Bush, R.I., Scherrer, P.H., Gummin, M.A., Smith, P., Auker, G., Jerram, P., Pool, P., Soufli, R., Windt, D.L., Beardsley, S., Clapp, M., Lang, J., Waltham, N.: 2012, The Atmospheric Imaging Assembly (AIA) on the Solar Dynamics Observatory (SDO). *Solar Phys.* **275**, 17. DOI. ADS.

Majumdar, S., Pant, V., Patel, R., Banerjee, D.: 2020, Connecting 3D evolution of coronal mass ejections to their source regions. *Astrophys. J.* **899**, 6. DOI. ADS.

Masson, S., McCauley, P., Golub, L., Reeves, K.K., DeLuca, E.E.: 2014, Dynamics of the transition corona. *Astrophys. J.* **787**, 145. DOI. ADS.

Michelson, A.A.: 1927, *Studies in Optics*, University of Chicago Press, Chicago. ISBN 9780226523880. books.google.co.in/books?id=FXazQgAACAAJ.

Morgan, H.: 2015, An atlas of coronal electron density at $5R_\odot$ I: Data processing and calibration. *Astrophys. J. Suppl.* **219**, 23. DOI.

Morgan, H., Byrne, J.P., Habbal, S.R.: 2012, Automatically detecting and tracking coronal mass ejections. I. Separation of dynamic and quiescent components in coronagraph images. *Astrophys. J.* **752**, 144.

Morgan, H., Druckmüller, M.: 2014, Multi-scale Gaussian normalization for solar image processing. *Solar Phys.* **289**, 2945. DOI. ADS.

Morgan, H., Habbal, S.R.: 2007, The long-term stability of the visible F corona at heights of 3–6 $R_\odot$. *Astron. Astrophys.* **471**, L47.

Morgan, H., Habbal, S.: 2010, A method for separating coronal mass ejections from the quiescent corona. *Astrophys. J.* **711**, 631. DOI. ADS.

Morgan, H., Habbal, S.R., Woo, R.: 2006, The depiction of coronal structure in white-light images. *Solar Phys.* **236**, 263. DOI. ADS.

Morrill, J.S., Korendyke, C.M., Brueckner, G.E., Giovane, F., Howard, R.A., Koomen, M., Moses, D., Plunkett, S.P., Vourlidas, A., Esfandiari, E., Rich, N., Wang, D., Thernisien, A.F., Lamy, P., Llebaria, A., Biesecker, D., Michels, D., Gong, Q., Andrews, M.: 2006, Calibration of the SOHO/LASCO C3 white light coronagraph. *Solar Phys.* **233**, 331. DOI. ADS.

Müller, D., St. Cyr, O.C., Zouganelis, I., Gilbert, H.R., Marsden, R., Nieves-Chinchilla, T., Antonucci, E., Auchère, F., Berghmans, D., Horbury, T.S., Howard, R.A., Krucker, S., Maksimovic, M., Owen, C.J., Rochus, P., Rodriguez-Pacheco, J., Romoli, M., Solanki, S.K., Bruno, R., Carlsson, M., Fludra, A., Harra, L., Hassler, D.M., Livi, S., Louarn, P., Peter, H., Schühle, U., Teriaca, L., del Toro Iniesta, J.C., Wimmer-Schweingruber, R.F., Marsch, E., Velli, M., De Groof, A., Walsh, A., Williams, D.: 2020, The solar orbiter mission. Science overview. *Astron. Astrophys.* **642**, A1. DOI. ADS.

Newkirk, G. Jr., Harvey, J.: 1968, Coronal polar plumes. *Solar Phys.* **3**, 321. DOI. ADS.

Owaki, N., Saito, K.: 1967, Photometry of the solar corona at the 1962 February eclipse. *Publ. Astron. Soc. Japan* **19**, 279. ADS.

Pasachoff, J.M., Rušin, V., Druckmuller, M., Saniga, M.: 2007, Fine structures in the white-light solar corona at the 2006 eclipse. *Astrophys. J.* **665**, 824. DOI.

Patel, R., K, A., Pant, V., Banerjee, D., K., S., Kumar, A.: 2018, Onboard automated cme detection algorithm for the visible emission line coronagraph on ADITYA-L1. *Solar Phys.* **293**, 103. DOI.

Patel, R., Pant, V., Chandrashekhar, K., Banerjee, D.: 2020, A statistical study of plasmoids associated with a post-CME current sheet. *Astron. Astrophys.* **644**, A158. DOI. ADS.

Patel, R., Pant, V., Iyer, P., Banerjee, D., Mierla, M., West, M.J.: 2021, Automated detection of accelerating solar eruptions using parabolic hough transform. *Solar Phys.* **296**, 31. DOI. ADS.

Qiang, Z., Bai, X., Ji, K., Liu, H., Shang, Z.: 2020, Enhancing coronal structures with radial local multi-scale filter. *New Astron.* **79**, 101383. DOI.

Raghavendra Prasad, B., Banerjee, D., Singh, J., Nagabhushana, S., Kumar, A., Kamath, P.U., Kathiravan, S., Venkata, S., Rajkumar, N., Natarajan, V., Juneja, M., Somu, P., Pant, V., Shaji, N., Sankarsubramanian, K., Patra, A., Venkateswaran, R., Adoni, A.A., Narendra, S., Haridas, T.R., Mathew, S.K., Krishna, R.M., Amareswari, K., Jaiswal, B.: 2017, Visible emission line coronagraph on ADITYA-L1. *Curr. Sci.* **113**, 613. DOI.

Renotte, E., Baston, E.C., Bemporad, A., Capobianco, G., Cernica, I., Darakchiev, R., Denis, F., Desselle, R., De Vos, L., Fineschi, S., Focardi, M., Górski, T., Graczyk, R., Halain, J.-P., Hermans, A., Jackson, C., Kintziger, C., Kosiec, J., Kranitis, N., Landini, F., Lédl, V., Massone, G., Mazzoli, A., Melich, R., Mollet, D., Mosdorf, M., Nicolini, G., Nicula, B., Orleański, P., Palau, M.-C., Pancrazzi, M., Paschalis, A., Peresty, R., Plesseria, J.-Y., Rataj, M., Romoli, M., Thizy, C., Thomé, M., Tsinganos, K., Wodnicki, R., Walczak, T., Zhukov, A.: 2014, ASPIICS: An externally occulted coronagraph for PROBA-3: Design evolution. In: Oschmann, J.M. Jr., Clampin, M., Fazio, G.G., MacEwen, H.A. (eds.) *Space Telescopes and Instrumentation 2014: Optical, Infrared, and Millimeter Wave*, *Proc. Soc. Photo-Opt. Instrum. Eng. (SPIE)* **CS-9143**, 91432M. DOI. ADS.

Seetha, S., Megala, S.: 2017, Aditya-L1 mission. *Curr. Sci.* **113**, 610. DOI.

Stenborg, G., Cobelli, P.J.: 2003, A wavelet packets equalization technique to reveal the multiple spatial-scale nature of coronal structures. *Astron. Astrophys.* **398**, 1185. DOI. ADS.

Stenborg, G., Vourlidas, A., Howard, R.A.: 2008, A fresh view of the extreme-ultraviolet corona from the application of a new image-processing technique. *Astrophys. J.* **674**, 1201. DOI. ADS.

Thernisien, A.: 2011, Implementation of the graduated cylindrical shell model for the three-dimensional reconstruction of coronal mass ejections. *Astrophys. J. Suppl.* **194**, 33. DOI. ADS.

Thernisien, A.F.R., Howard, R.A., Vourlidas, A.: 2006, Modeling of flux rope coronal mass ejections. *Astrophys. J.* **652**, 763. DOI. ADS.

Thernisien, A., Vourlidas, A., Howard, R.A.: 2009, Forward modeling of coronal mass ejections using STEREO/SECCHI data. *Solar Phys.* **256**, 111. DOI. ADS.

Thompson, W.T., Wei, K., Burkepile, J.T., Davila, J.M., St. Cyr, O.C.: 2010, Background subtraction for the SECCHI/COR1 telescope aboard STEREO. *Solar Phys.* **262**, 213. DOI. ADS.

van de Hulst, H.C.: 1950, The electron density of the solar corona. *Bull. Astron. Inst. Neth.* **11**, 135.

Woo, R.: 2005, Relating white-light coronal images to magnetic fields and plasma flow. *Solar Phys.* **231**, 71. DOI. ADS.

Authors and Affiliations

Ritesh Patel[1,2,3] (iD) · **Satabdwa Majumdar**[1,4] (iD) · **Vaibhav Pant**[2] (iD) ·
Dipankar Banerjee[1,2,5] (iD)

✉ D. Banerjee
  dipu@iiap.res.in

  V. Pant
  vaibhav.pant@aries.res.in

[1]   Indian Institute of Astrophysics, Koramangala, Bengaluru, 560034, India

[2]   Aryabhatta Research Institute of Observational Sciences, Nainital, 263001, India

[3]   University of Calcutta, 87/1, College Street, Kolkata, 700073, India

[4]   Pondicherry University, Chinna Kalapet, Kalapet, Puducherry, 605014, India

[5]   Center of Excellence in Space Sciences, IISER, Kolkata, 741246, India